METALS AND MATERIALS International, Vol. 9, No. 4 (2003), pp. 399~404

An Electrochemical Etching Procedure for Fabricating Scanning Tunneling Microscopy and Atom-Probe Field-Ion Microscopy Tips

Yeong-Cheol Kim[1,*] and David N. Seidman[2]

[1] Department of Materials Engineering, Korea University of Technology and Education
P.O. Box 55, Cheonan 330-708, Korea
[2] Department of Materials Science and Engineering and Materials Research Center
R. R. McCormick School of Engineering and Applied Science, Northwestern University
2225 N. Campus Drive, Evanston, IL 60208-3108, USA

A two-step electrochemical etching procedure is developed to control the sharpness and shape of tips used for either scanning tunneling microscopy (STM) or atom-probe field-ion microscopy (APFIM). The formation of a neck near a tip's apex is controlled by carefully limiting the amount of chemical solution in contact with the area of the neck. Reproducible, atomically sharp, and appropriately tapered tips can be manually produced with this procedure.

Keywords: tips, STM, FIM, electrochemical etching

1. INTRODUCTION

Electrochemical etching procedures are commonly employed to fabricate scanning tunneling microscopy (STM) or atom-probe field-ion microscopy (APFIM) tips. Since electrochemical etching procedures involve immersing the tip in chemical solutions and exposing the tip to air, deposited reaction by-products and surface oxides are often found on the surface of a tip. Both the surface oxides and deposited by-products must be removed to reduce noise levels in STM images and APFIM time-of-flight spectra. As a result, it is necessary to treat subsequently the tips *in situ* or *ex situ*. Typically, controlled deposition on the top plane of a tip's apex [1], controlled collision of the apex of a tip with a clean metal/semiconductor surface [2], and field-evaporation at elevated temperatures employing a highly controlled applied electric field [3] have been utilized to obtain atomically sharp STM tips. To maximize the probability of producing a usable tip by these methods, the initial electrochemical procedure must generate sharp tip's with the desired shape. The shape of a tip is expressed by the aspect ratio, ξ, which is given by the ratio of a tips length to its shank angle. To minimize flexural vibrations, tips with small values of the aspect ratio, ξ, are required for STM; while to maximize the number of atoms analyzed in an APFIM data set, tips with high values of ξ are required - the larger the better.

*Corresponding author: yckim@kut.ac.kr

Extensive research has been devoted to obtaining sharp tips by means of electrochemical etching techniques [4-13]. In the standard electrochemical etching procedure the duration of time when a tip is atomically sharp is very short (less than submicroseconds). The main experimental challenge is to halt all reactions at the moment a tip is atomically sharp. Changes in electrolyte composition, concentration, and temperature, as well as the applied voltage and polarity (dc or ac) have been studied in order to control quantitatively the etching rate and to improve the ability to stop the reactions. Ibe *et al.* [4] introduced a high-speed electromechanical switch to stop the etching reaction at the correct time. To avoid excessive blunting of APFIM tips, Krakauer *et al.* [14] monitored the tip diameter and ξ employing transmission electron microscopy (TEM) between msec voltage pulses, during the final stages of the tip sharpening process; they utilized a specially fabricated double-tilt axis TEM holder, that can hold 1 cm long wires to observe the aspect ratio, ξ. Bryant *et al.* [10] collected the normally discarded immersed portion of the wire and employed it as an STM tip, based on the reasoning that etching stops the moment the immersed section separates from the wire. Weinstein *et al.* [5] and Bourque *et al.* [12] used an inert mask to limit contact of the tip with the chemical electrolyte after the wire necks and separates into two portions. Fotino [8] intentionally introduced gas bubbles to limit the reaction between the apex of the tip and the chemical electrolyte; unfortunately, the tip's surfaces were found to be ragged due to inhomogeneous

protection by gas bubbles. These methods have all had some degree of success in obtaining atomically sharp tips, but they lack the capability of controlling the aspect ratio, ξ.

In this paper, we first revisit the electrochemical etching mechanism of tungsten in a NaOH aqueous solution to point out an incorrect concept that has been accepted in literature, and to estimate the radius change rate, (dr_n/dt), of the tungsten wire during the final critical etching period. With this background material, we report on an electrochemical etching procedure that can control both a tip's sharpness and geometry, ξ, by reducing the reaction rate at the final stage of the tip sharpening process. We present sample results of this procedure for tungsten, since it is the most widely used material for STM tips and has also been studied extensively by APFIM, although the procedure can be extended to any other tip material.

2. ELECTROCHEMICAL ETCHING PROCEDURE

The electrochemical etching of tungsten in an aqueous solution involves its anodic dissolution [15,16]. The basic electrochemical reactions are [17]:

cathode

$$2H_2O+2e^- \leftrightarrow H_2(g)+2OH^- \qquad E_c^o = -0.83\ V \qquad (1)$$

anode

$$W(s)+8OH^- \leftrightarrow WO_4^{2-}+4H_2O+6e^- \quad E_a^o = +1.05\ V \qquad (2)$$

and the overall reaction is obtained by adding three times Eqs. 1 to 2 to obtain:

overall

$$W(s)+2OH^-+2H_2O \leftrightarrow WO_4^{2-}+3H_2(g) \quad E^o = +0.22\ V \qquad (3)$$

The positive value for the overall standard electrode potential, E^o, indicates that the direction of the overall reaction is forward from left to right, Eq. 3, under standard conditions [18]. In obtaining the overall reaction, the standard electrode potential of the cathode, E_c^o, should not be multiplied by 3, since it is a size-independent intrinsic parameter. This error was made in Ref. 4, and propagated to other publications [19]. And this error affects the estimate of the stability of tungsten in a fresh NaOH chemical solution, since the sign of the overall standard electrochemical potential, E^o, is changed from positive to negative. The stability of tungsten in the NaOH chemical solution is discussed employing the corrected expression for the electrochemical potential, E, in the next section.

The electrochemical potential, E, for the overall reaction is

$$E = +0.22 - \frac{RT}{nF}\ln\left(\frac{[WO_4^{2-}]\cdot P_{H_2}^3}{[OH^-]^2}\right) \qquad (4)$$

where R is the ideal gas constant, T is temperature, n is the number of electrons involved in the overall reaction, and F is Faraday's constant. For a fresh 2N NaOH solution, the concentration of tungstate ions (WO_4^{2-}) is initially negligible and, therefore, the second term on the right-hand side of the Eq. 4 is negative; thus, the value of E is greater than +0.22 V at the beginning of the electrochemical reaction. Thermodynamically, the dissolution of tungsten is favored, and occurs without an externally applied voltage. Typically, however, the dissolution rate of a tungsten wire placed in an electrolytic solution, without an applied voltage, is quite small. Nevertheless, even slow dissolution rates are detrimental to obtaining atomically sharp tips, since any amount of dissolution in the area of the tip destroys its atomic sharpness. This is the reason why electrochemically etched sharp tips should be immediately taken out of the chemical solution and rinsed in triply distilled water or pure ethyl alcohol. Over time, however, due to an accumulation of tungstate ions (WO_4^{2-}) and decreased hydroxide (OH^-) concentrations, the second term on the right-hand side of the Eq. 4 can become positive. For sufficiently old electrolytic solutions, the intrinsic electrochemical potential may approach or pass zero. This could prevent blunting of the tip by reducing or eliminating any intrinsic electrochemical driving force for dissolution while the tip is in the electrolyte.

Fig. 1(a) is a schematic diagram of an electrochemical etching cell showing a tungsten anode being etched in a NaOH solution, with an applied dc voltage between the cathode and anode that drives the etching process. A 5 mm diameter stainless steel ring placed around the anode serves as the cathode. Fig. 1(b) schematically indicates the etching mechanism. The heavy tungstate ions flow down the sides of the wire, resulting in an inflow of fresh solution to it. The fresh

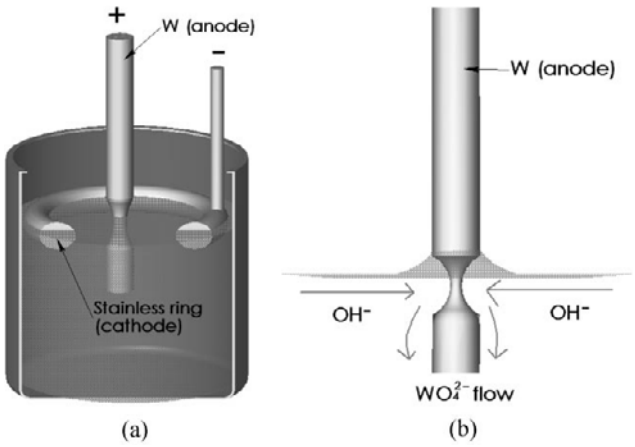

Fig. 1. (a) Schematic diagram of an electrochemical cell displaying the dissolution of a tungsten wire (anode) in a NaOH solution when a dc voltage polarity is applied to the cell. (b) A schematic illustration of the etching mechanism showing the flow of tungstate ions down the sides of wire and subsequent inflow of fresh electrolyte containing OH^- ions.

solution, containing OH^- ions, impinges on the wire at or just below the solution's surface, where the path to the anode is not retarded by the downward flow of the tungstate ions. The flow of tungstate ions also tends to retard the etching rate of the wire below the surface, by hindering the drift of fresh OH^- ions from the bulk of the solution to the wire's surface. The readily observable turbulence at a tungsten anode near the solution's surface, due to the inflow of fresh fluid, enhances the reaction in this area, resulting in the commonly observed formation of a neck.

If the applied voltage is ac, then the tungsten electrode alternates between being the cathode and anode. During the portion of the cycle when the tungsten is the cathode, hydrogen bubbles are generated via the reaction given by Eq. 1. Tungstate ions generated during the positive half cycle are expelled from the tungsten electrode during the negative half of the cycle. This, combined with the turbulence generated from the hydrogen gas produced, helps to remove the tungstate ions from the tungsten surface and supply the hydroxide ions to it. Therefore, the reaction rate employing an ac voltage polarity is much faster than that with dc voltage polarity. Since the electric field-driven repulsive force is higher at sharper geometries, the surfaces on the bottom perimeter of the immersed tungsten wire initially have the highest etching rate. The result is a smooth and nicely tapered tip with the commonly observed cone shape. It is hard, however, to obtain atomically sharp tips with an ac voltage, as the tip forms at the bottom of the immersed portion, and tends to blunt extremely fast due to the high local electric field and the absence of a diffusion barrier from the tungstate ions surrounding the wire.

We now model the etching process to estimate the etching rate for the dc voltage polarity case. It is assumed that the dominant flux of OH^- ions to the tungsten anode is due to the drift term caused by the dc voltage between the cathode, where the OH^- ions are created, and the anode; that is, we neglect the concentration gradient, if any, in the OH^- ion concentration. We also assume that etching rate is diffusion-limited and not interface-limited. This is a reasonable assumption as W reacts with OH^- ions to form WO_4^{2-} ions that flow rapidly downward along the bottom portion of the wire (see Eq. 4 and Fig. 1) and therefore do not hinder the reaction of W with OH^- ions in the neck region. The Nernst-Einstein drift velocity, $\vec{v}$, for the OH^- ions is

$$\vec{v} = e\mu\vec{E} \tag{5}$$

where e is the charge on an electron, μ is the ion mobility, and $\vec{E}$ is the electric field between the cathode and anode. Thus the expression for $\vec{v}$ in the electrolyte is

$$\vec{v} = -\frac{De\vec{E}}{kT} \tag{6}$$

where D is the diffusivity of OH^- in the electrolyte, and kT has its usual significance. For the geometry of our electrochemical cell the estimated value of $\vec{v}$ is approximately 1 cm sec^{-1} from Eq. 6. The etching rate, dr_n/dt, in the neck region is obtained by equating the number of tungsten atoms removed per cm^3, [W], when the wire's radius shrinks by the increment, dr_n, to the inward flux (cm^{-2} sec^{-1}) of hydroxide ions, J_{OH^-}, in the corresponding time, dt. Thus the expression for this mass balance is

$$[W]dr_n = J_{OH^-}dt \tag{7}$$

The quantity J_{OH^-} is given by the product of the OH^- concentration, $[OH^-]$, and the drift velocity given by Eq. 6; note that for every two OH^- ions that arrive at the anode one tungsten atom is removed (Eq. 3). Thus the expression for dr_n/dt is

$$-\left(\frac{dr_n}{dt}\right) = \frac{2[OH^-]De\vec{E}}{[W]kT} \tag{8}$$

The equation for $\vec{E}$ is approximately that for a cylindrical capacitor geometry and it depends inversely on r; the origin is in the center of the anode wire. Thus if all the terms in Eq. 8 are taken to be constant except r we obtain

$$-\left(\frac{dr_n}{dt}\right) = \frac{K}{2r} \tag{9}$$

Eq. 9 is readily integrated, with the condition that r_n is initially r_{no}, to obtain

$$r_n^2(t) = r_{no}^2 - Kt \tag{10}$$

which predicts that neck radius, $r_n(t)$, decreases parabolically with increasing time. Therefore, Eq. 10 can be used to estimate the etching rate constant, K. When r_{no} is 0.25 mm, it takes 22 min. to complete the tip sharpening procedure employing a dc voltage polarity. Hence, the value of K is 5×10^{-5} mm^2 sec^{-1} based on the above experimental data.

Fig. 2 displays (dr_n/dt) as a function of the inverse radius, r_n^{-1}. The value of (dr_n/dt) approaches infinity, of course, as the radius approaches zero. Therefore, a short response time is essential for fabricating sharp tips. When K is an order of magnitude smaller than the previous value, (dr_n/dt) decreases significantly slower in the thin neck region. The value of K must be much larger when an ac voltage polarity is employed, resulting in a huge (dr_n/dt) value in the final stage of the tip sharpening process. The vertical line indicates a neck radius of 20 nm, where the applied tensile stress, due to the portion of the wire below the neck, exceeds the mechanical yield strength (1920 MPa) of a tungsten crystal [20]. The tensile force (mg) due to the mass, m, (where g is the acceleration due to gravity) of the lower portion of the immersed wire is estimated by taking the immersed length to be 1 mm, its ini-

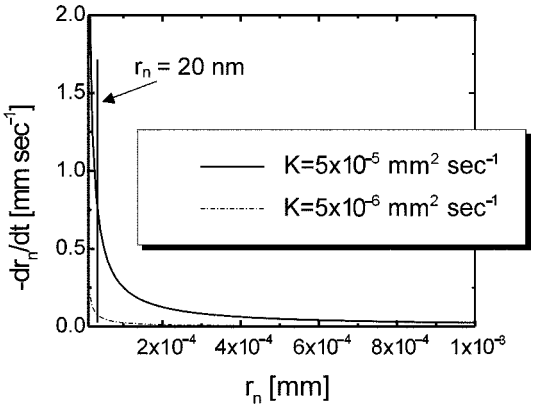

Fig. 2. The radius change rate, (dr_n/dt), as a function of the inverse radius, r_n^{-1}. Two different values for K are employed to estimate the radius change rate. The vertical line indicates a neck radius, r_n=20 nm, where the applied tensile stress due to the lower portion of the necked region exceeds the mechanical tensile strength of a tungsten crystal specimen.

tial diameter to be 0.25 mm, and the final diameter to be 0.125 mm (50 % of the initial diameter). These numbers are experimentally obtained from our research and ref. 4. The actual critical neck radius is less than this estimated value since the probability of having an operative dislocation source in this thin neck region is small and, therefore, the tungsten's yield strength approaches the theoretical value of ≈G/20; where G is the shear modulus and its value is 160.2 GPa for tungsten at room temperature [21]. The calculated critical neck radius based on this value of the shear modulus is 5 nm. The optimum technique involves stopping the reaction the moment the cross-sectional area of the neck is close as possible to zero.

3. EXPERIMENTAL PROCEDURE

We now describe a two-step simple electrochemical etching procedure for obtaining atomically sharp STM or APFIM tips based on the information presented in the previous section concerning the electrochemical reaction mechanism. The electrochemical etching procedure shown in Fig. 1, that we used for a while, suffers from an inability to obtain reproducibly sharp tips, due to the high neck radius rate of change in the final stage of the etching procedure. The main idea of this new procedure is to decrease the etching rate significantly in the area of the tip by controlling its geometry. Therefore, the period of time a tip is atomically sharp is sufficiently long to allow manually switching off the etching process.

First, a wire-shaped starting material is tapered via a beaker etching procedure (Ref. 14) in a setup that is similar to Fig. 1. The main objective of this step is to decrease a thick starting wire (~300 micron diameter) to a thin taper (~10 micron diameter) by employing a high etching rate, which is

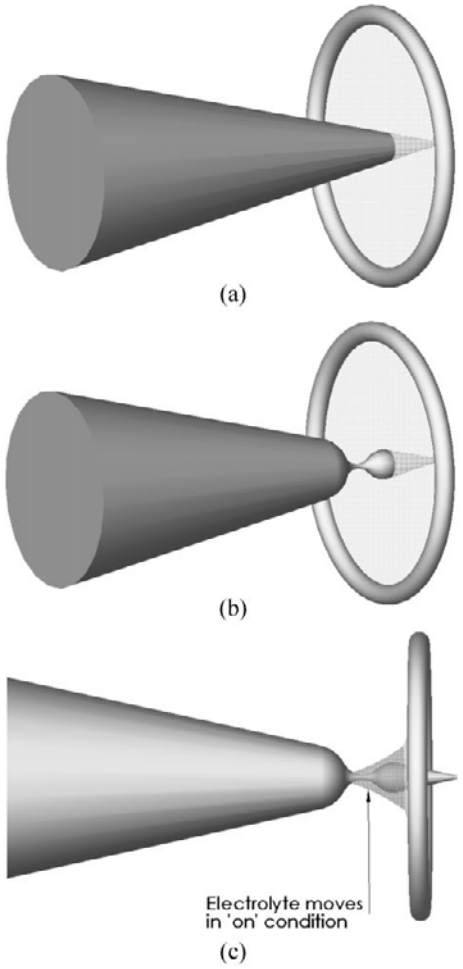

Fig. 3. Schematic diagram of loop etching procedure. (a) The tapered wire from the beaker etching procedure is inserted deep enough into the meniscus, containing the electrolyte, to expose its end portion to air. (b) The end portion alone is immersed into the chemical solution after the neck is formed in Fig. 3(a). (c) During the 'on' period of the etching process, the chemical solution moves to the unwetted neck area.

achieved by using ac voltage polarity. Since the highest etch rate occurs at the bottom of the tungsten anode, this procedure produces a well-tapered tungsten wire as shown in Fig. 3(a). The tip, however, is not sharp as explained in the previous section.

For the second part of the procedure the tapered wire is moved to an electrolytic cell in the form of a loop as shown in Fig. 3(a). Further sharpening of the tip is performed using this loop with dc voltage polarity. The etching rate is reduced by diluting the active element from 2N NaOH to 0.2N NaOH, in the electrochemical solution, to increase the period of time a tip is atomically sharp. The loop etching procedure is monitored via an optical microscope. During the initial period when the tip diameter is greater than 1 micron, a low magnification (50×) is used to observe the etching procedure. The tapered tip is inserted deep enough into the electrolyte, which is in the form of a meniscus, to expose its end. When

the etching procedure is initiated, a small amount of electrochemical solution wets the unwetted end of the tip. The etching rate, however, at the end portion of the taper is much lower than at the part immersed in the electrochemical solution. Therefore, the etching procedure produces a neck near the end portion, as shown in Fig. 3(b). When the thickness of the neck is about one-half of that of the end portion, the entire portion, including the neck and end portions, is immersed in the chemical solution and polished until the area of the neck is optically transparent at a magnification of 50. The etching process is intermittently stopped by taking the immersed portion out of the chemical solution to measure the neck's thickness. The configuration shown in Fig. 3(a) can be reemployed to control the shape of a neck. When the region of the neck is optically transparent, the end portion alone is immersed in the electrochemical solution as indicated in Fig. 3(b). Then the magnification is increased to 200 to observe the thinned area of the neck, and when it is optically transparent at this magnification the neck radius is usually less than 100 nm. The voltage can be further reduced to slow down the reaction rate. Short pulses with a width of less than one microsecond, generated by a specially fabricated pulse generator [14], are used to reduce the etching rate. Even though there is no chemical solution wetting of the area of the neck during the 'off' period, the chemical solution moves to the unwetted neck area, as shown in Fig. 3(c), during the on period. Manual control with an on/off switch, that has a typical switching time of 10 msec, is sufficient to obtain sharp tips employing this configuration. This is because the etching rate in region of the neck is significantly lower than that of the immersed portion, as the tip geometry serves as a barrier to the chemical solution.

4. RESULTS

Fig. 4 exhibits a scanning electron micrograph of a tungsten tip with a neck. The length of the end portion can be reduced further by selectively etching it employing the configuration displayed in Fig. 3(b). The etching rate in the area of the neck can be further reduced by forming two necks or even three necks to limit the access of the chemical solution to the neck area of interest. We have also fabricated sharp tips from iron-based alloys with a high aspect ratio, ξ, for APFIM experiments [22].

Fig. 4. A scanning electron microscope (SEM) micrograph of a tungsten tip with a neck recorded employing a Hitachi S570 at 28 kV.

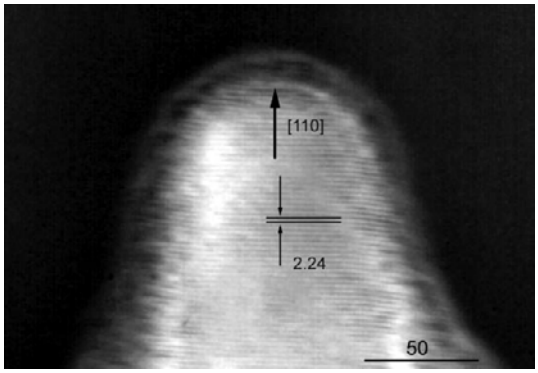

Fig. 5. A high resolution electron micrograph of a tungsten tip. The {110}-type planes perpendicular to the long axis of the tip are clearly resolved. This image was recorded employing a Hitachi 8100.

Fig. 5 is a high resolution electron microscope (HREM) micrograph exhibiting a sharp tungsten tip after completion of the etching procedure. The tip diameter is about 10 nm and the atomic planes resolved edge-on are the {110}-type. The halo surrounding the tip is an amorphous carbon layer that formed during observation of the tip in the HREM.

Fig. 6 is an STM image of a Si {111}-type 7×7 surface

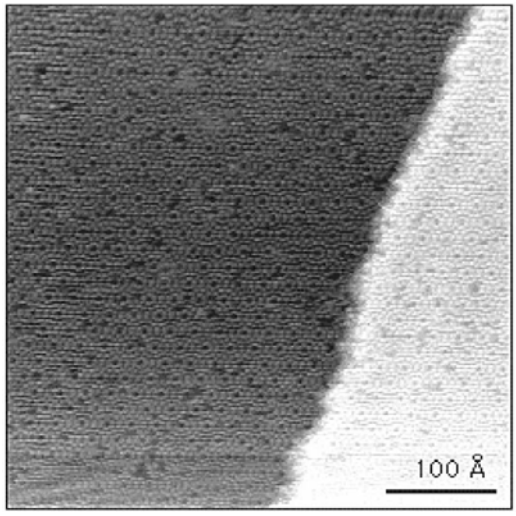

Fig. 6. An atomic resolution scanning tunneling microscope image of a Si {111}-type 7×7 structure. The scanned area is 50 nm×50 nm and the black to white scale is 1.5 nm. This image was recorded employing an Omicron ultrahigh vacuum compact scanning tunneling microscopy/atomic force microscopy system.

resolved employing a tungsten tip prepared by the etching procedure described in this paper. There is height shift in the lower portion of this image, which we think is due to an atomic configuration change on the tip's apex during scanning. This is not surprising, when one notes the high surface diffusivity of a tungsten atom on a tungsten {110}-type plane at room temperature [23]. The estimated value of the root-mean-squared surface diffusion distance of a tungsten atom on a {110}-type plane of tungsten at room temperature during the course of a one minute scan is about 0.2 nm. The height difference between the two terraces is about 1 nm. The distortions in the top and bottom portions of the image are due to a hysteresis effect of the piezoelectric material employed as a scanner. There are identifiable point defects in the Si {111}-type 7×7 surface image which have been ascribed to oxygen atoms or silicon vacancies that are present after a surface heat treatment, or hydrogen atoms adsorbed from the ambient pressure in a stainless steel ultrahigh vacuum chamber [24,25].

5. CONCLUSIONS

The conventional electrochemical etching mechanism for tungsten scanning tunneling microscopy (STM) or atom-probe field-ion microscopy (APFIM) tips is reviewed, and it is found that controlling the neck radius change rate, (dr_n/dt), at the final stage of the etching procedure is critical for obtaining atomically sharp tungsten scanning tunneling microscopy (STM) or atom-probe field-ion microscopy (APFIM) tips. Based on this fact a two-step electrochemical etching procedure is developed to control tip sharpness and shape. Neck formation near the apex of a tip is controlled by limiting the amount of chemical solution in contact with the area of the neck. Reproducible, atomically sharp, and appropriately tapered tips can be manually produced with this procedure. It is applied to imaging a Si {111}-type 7×7 structure.

ACKNOWLEDGMENT

This research was funded by the National Science Foundation through a grant to the Materials Research Center at Northwestern University.

REFERENCES

1. H. W. Fink, *IBM J. Res. Develop.* **30**, 460 (1986).
2. *Private Communication with Prof. Jun Nogami*, University of Wisconsin-Milwaukee.
3. V. T. Binh, *J. Microscopy* **152**, 355 (1988); V. T. Binh, *Surf. Sci.* **202**, L539 (1988).
4. J. P. Ibe, P. P. Bey, Jr., S. L. Brandow, R. A. Brizzolara, N. A. Burnham, D. P. DiLella, K. P. Lee, C. R. K. Marrian, and R. J. Colton, *J. Vac. Sci. Tech. A* **8**, 3570 (1990).
5. V. Weinstein, M. Slutzky, A. Arenshtam, and E. Ben-Jacob, *Rev. Sci. Instrum.* **66**, 3075 (1995).
6. S. F. Ceballos, G. Mariotto, S. Murphy, and I. V. Shvets, *Surf. Sci.* **523**, 131 (2003).
7. R. Nicolaides, Y. Liang, W. E. Packard, Z. Fu, H. A. Blackstead, K. K. Chin, John D. Dow, J. K. Furdyna, W. M. Hu, R. C. Jaklevic, W. J. Kaiser, A. R. Pelton, and M. V. Zeller, *J. Vac. Sci. Tech. A* **6**, 445 (1988).
8. M. Fotino, *Rev. Sci. Instrum*. **64**, 159 (1993).
9. A. Cricenti, E. Paparazzo, M. A. Scarselli, L. Moretto, and S. Selci, *Rev. Sci. Instrum.* **65**, 1558 (1994).
10. P. J. Bryant, H. S. Kim, Y. C. Zheng, and R. Yang, *Rev. Sci. Instrum.* **58**, 1115 (1987).
11. R. Guckenberger, C. Kosslinger, R. Gatz, H. Breu. N. Levai, and W. Baumeister, *Ultramicroscopy* **25**, 111 (1988).
12. H. Bourque and R. M. Leblanc, *Rev. Sci. Instrum.* **66**, 2695 (1995).
13. L. Libioulle, Y. Houbion, and J. M. Gilles, *Rev. Sci. Instrum.* **66**, 97 (1995).
14. B. W. Krakauer and D. N. Seidman, *Rev. Sci. Instrum.* **63**, 4071 (1992); B. W. Krakauer, J. G. Hu, S. M. Kuo, R. L. Mallick, A. Seki, D. N. Seidman, J. P. Baker, and R. Loyd, *Rev. Sci. Instrum.* **61**, 3390 (1990).
15. J. W. Johnson and C. L. Wu, *J. Electrochem. Soc.* **118**, 1909 (1989).
16. G. S. Kelsey, *J. Electrochem. Soc.* **124**, 814 (1977).
17. W. M. Latimer, *The Oxidation States of the Elements and Their Potentials in Aqueous Solutions*, p. 32, Prentice-Hall, Englewood Cliffs (1952).
18. W. J. Moore, *Physical Chemistry*, p. 473, Prentice-Hall, Englewood Cliffs (1958).
19. C. J. Chen, *Introduction to Scanning Tunneling Microscopy*, Chap. 13, Oxford University Press, New York (1993); R. Zhang and D. G. Ivey, *J. Vac. Sci. Tech. B* **14**, 1 (1996).
20. *Goodfellow Catalog*, p. 31 (1995/1996).
21. D. I. Bolef and J. de Kleark, *J. Appl. Phys.* **33**, 2311 (1962).
22. Y. C. Kim, C. J. Yu, and D. N. Seidman, *J. Appl. Phys*. **81**, 944 (1997).
23. G. Ehrlich and F. G. Hudda, *J. Chem. Phys.* **44**, 1036 (1966); T. T. Tsong, *Phys. Rev. B* **6**, 417 (1972); G. L. Kellogg, *Surf. Sci. Rep*. **21**, 1 (1994).
24. T. Sakurai, Y. Hasegawa, T. Hashizume, I. Kamiya, T. Ide, I. Sumita, H. W. Pickering, and S. Hyodo, *J. Vac. Sci. Tech. A* **8**, 259 (1990).
25. Y. Kobayashi and K. Sugii, *J. Vac. Sci. Tech. B* **9**, 748 (1991).